Supporting Information for "Shared control of gene expression in bacteria by transcription factors and global physiology of the cell"

Sara Berthoumieux, Hidde de Jong, Guillaume Baptist, Corinne Pinel
Caroline Ranquet, Delphine Ropers, Johannes Geiselmann

Contents

S1 Strains and plasmids

The *E. coli* strains used in this study are the wild-type strain BW25113 as well as the Δ*fis*, Δ*crp*, and Δ*cya* deletion mutants of BW25113. The Δ*fis* and Δ*cya* mutants were taken from the Keio collection (Baba et al., 2006), whereas the Δ*crp* mutant was reconstructed

in our laboratory (Baptist et al., 2012). The reconstruction was necessary because the Δ*crp* deletion mutant in the Keio collection was incorrect (Yamamoto et al., 2009) (Table S1).

Strains	Characteristics	Reference or source
WT	*E. coli* BW25113	(Baba et al., 2006)
Δ*fis*	*E. coli* BW25113 Δ*fis*	(Baba et al., 2006)
Δ*crp*	*E. coli* BW25113 Δ*crp*	(Baptist et al., 2012)
Δ*acs*	*E. coli* BW25113 Δ*acs*	(Baba et al., 2006)

Table S1: Strains used in this study.

The wild-type and mutant strains were transformed with plasmids bearing a *gfp* reporter gene (Table S2). The standard backbone used is the pZE*gfp* plasmid, possesses a colE1 origin of replication, and has the ampicillin resistance marker *bla*. The plasmid is present at about thirty copies per cell, carries the coding sequence of the fast-folding and short-lived GFPmut3 reporter, and does not affect bacterial growth (de Jong et al., 2010). The specific advantages of this reporter system for our study are that it generally produces a strong signal, well beyond the auto-fluorescence background, and that the short half-life (58 min) and maturation time (25 min) of the GFP allows the dynamics of the promoter activity to be followed in real time. We constructed transcriptional fusions by cloning the promoter region of the genes *fis*, *crp*, and *rpoS*, as well as the synthetic promoter ptet (Lutz and Bujard, 1997), into the pZE*gfp* plasmid backbone. The primers used for the reporter plasmids constructed in this study are shown in Table S3. The constructions were verified by sequencing. A pZE*gfp* reporter for the pRM promoter of phage λ was obtained from Michael Elowitz (Elowitz and Leibler, 2000).

Plasmid	Characteristics	Reference or source
pZE*gfp*	Amp^r, colE1 *ori*, *gfpmut3*	(de Jong et al., 2010)
pZE1RM*gfp*	Amp^r, colE1 *ori*, p*RM-gfpmut3*	(Elowitz and Leibler, 2000)
pZE*fis-gfp*	Amp^r, colE1 *ori*, p*fis-gfpmut3*	(de Jong et al., 2010)
pZE*crp-gfp*	Amp^r, colE1 *ori*, p*crp-gfpmut3*	This study
pZE*rpoS-gfp*	Amp^r, colE1 *ori*, p*rpoS-gfpmut3*	This study
pZEptet-*gfp*	Amp^r, colE1 *ori*, ptet-*gfpmut3*	This study
pUA66*gfp*	Kan^r, pSC101 *ori*, *gfpmut2*	(Zaslaver et al., 2006)
pUA66*acs-gfp*	Amp^r, pSC101 *ori*, p*acs-gfpmut2*	(Baptist et al., 2012)

Table S2: Plasmids used in this study.

In the case of *acs*, we did not succeed in constructing a pZE*gfp* reporter. We therefore selected a reporter for this gene from the plasmid library developed by the Alon group (Zaslaver et al., 2006). It consists of a transcriptional fusion of the promoter region of *acs* with the *gfp* gene encoding the fast-folding and long-lived GFPmut2 reporter, carried on a pUA66*gfp* plas-

Plasmid	Primer sequence
pZE*crp-gfp*	crp1: CTG GGA ATT CGC TAT CAA CTG TAC TGC crp2: CAT GCT CGA GCG AGA CAC CAG GAG
pZE*rpoS-gfp*	rpoS1: GCT GGC TCG AGA CGT GAG GAA ATA C rpoS2: CGG AGA ATT CAA GCA AAA GCC TG
pZEptet-*gfp*	pZE-ptet1: TCT CTA TCA CTG ATA GGG ACT TTA CCT CTG GCG GTG ATA G pZE-ptet2: ATC AGC AGG ACG CAC TGA CCG AAT TCA TTA AAG AGG AGA A ptet1: CCT ATC ACC GCC AGA GGT AAA GTC CCT ATC AGT GAT AGA GAT TGA CAT CCC TAT CAG TGA TAG AGA TAC TGA GCA CAT CAG CAG GAC GCA CTG ACC GAA TTC ATT AAA GAG GAG AA ptet2: TTC TCC TCT TTA ATG AAT TCG GTC AGT GCG TCC TGC TGA TGT GCT CAG TAT CTC TAT CAC TGA TAG GGA TGT CAA TCT CTA TCA CTG ATA GGG ACT TTA CCT CTG GCG GTG ATA GG

Table S3: Primers used for the construction of strains pZE*crp-gfp*, pZE*rpoS-gfp*, and pZEptet-*gfp*. We have amplified the promoter regions of *crp* and *rpoS* by PCR from genomic DNA of *E. coli*, with oligonucleotides Crp1/Crp2 and RpoS1/RpoS2, respectively. Oligonucleotides RpoS1 and Crp2 contain an XhoI restriction site, and oligonucleotides RpoS2 and Crp1 an EcoRI restriction site, which allows cloning of the amplified DNA between these two sites on the pZE*gfp* plasmid. pZEptet-*gfp* was constructed with the Gibson Assembly method (Gibson, 2011). The pZE*gfp* plasmid backbone was amplified by means of primers pZE-ptet1 and pZE-ptet2. The ptet promoter was directly synthesized by annealing two complementary long primers (ptet1 and ptet2).

mid. This vector has the origin of replication of the pSC101 plasmid, is present below 5 copies per cell, and has a different resistance marker (*kan*). In order to transform pUA66*acs-gfp* into the BW25113 deletion strains, we replaced the kanamycin by the ampicillin resistance marker. In the data analysis, as explained in Sec. S2 and Sec. S8, we corrected for other differences between the two vectors (GFP half-life, maturation, and plasmid copy number variation).

The promoterless vectors pZE*gfp* and pUA66*gfp* were used for background correction (Sec. S2). In our conditions, the two strains have practically identical growth curves and fluorescence signals, and their promoter kinetics are undistinguishable from the wild-type BW25113 strain.

S2 Computation of promoter activities from reporter gene data

In order to monitor gene expression *in vivo* and in real time, we used fluorescent reporter genes in combination with automated microplate readers. The reporter gene experiments produce about 120 measurements of absorbance (600 nm) and fluorescence (485-520 nm) during a typical acquisition period (about 10 h). The absorbance or optical density is a measure of the biomass of a bacterial population. It can be used to estimate the total volume of bacterial cells in a population over a large range of growth rates (Volkmer and Heinemann, 2011). The fluorescence emitted is proportional to the quantity of GFP in the cell population. The absorbance is expressed in dimensionless units, whereas fluorescence intensities are reported in relative fluorescence units (RFU).

The primary data are corrected for background levels of absorbance and fluorescence. For the absorbance background, we use wells in the microplate containing growth medium only, that is, without bacterial cells. Denoting by $a_u(t)$ the uncorrected absorbance at time t and by $a_b(t)$ the background absorbance, the corrected absorbance $a(t)$ is given by

$$a(t) = a_u(t) - a_b(t). \tag{S1}$$

The fluorescence background is determined by performing measurements on a strain carrying the promoterless vector, that is, a strain with a nonfunctional reporter system. Contrary to the absorbance, the fluorescence background is not constant, but varies with the population size due to the autofluorescence of cells. Since the growth curves of the reporter strain and the strain with the nonfunctional reporter system are not necessarily identical, we cannot simply subtract the background readings at each time-point. We therefore developed a calibration curve relating absorbance readings to background fluorescence levels.

Let $a_u(t)$ and $f_u(t)$ denote the uncorrected absorbance and fluorescence at time t, respectively, for bacteria carrying the functional reporter plasmid. Similarly, let $b_u(t)$ and $g_u(t)$ denote the uncorrected absorbance and fluorescence, respectively, for bacteria carrying the promoterless reporter plasmid. We call β the empirical function relating $b_u(t)$ to $g_u(t)$, that is, $g_u = \beta(b_u(t))$. The function β is obtained in our case by non-parametric regression using smoothing splines (MATLAB). By means of this calibration curve, the corrected absorbance is defined as

$$f(t) = f_u(t) - \beta(a(t)). \tag{S2}$$

Fig. S1*A-D* shows an example of background correction, applied to fluorescence data acquired for the gene *fis* in a wild-type BW25113 strain. The fluorescence background correction procedure described above was slightly modified from the one we used in previous work (Boyer et al., 2010; de Jong et al., 2010). The modifications take into account the fact that part of the fluorescence background is contributed by the growth medium, that is, the background levels do not approach 0 for small absorbance values.

In the remainder of this section, we explain how the absorbance and fluorescence measurements can be related to biologically relevant quantities, in particular promoter activities. Following (Boyer et al., 2010; de Jong et al., 2010), we develop a simple kinetic model describing the expression of the reporter gene. Let $x_g(t)$ [μM] denote the time-varying concentration of GFP in the cells in the population. The dynamics of $x_g(t)$ is defined by the differential equation

$$\frac{dx_g(t)}{dt} = p(t) - (\mu(t) + \gamma_g)\, x_g(t), \tag{S3}$$

where $p(t)$ [μM $\quad \min^{-1}$] represents the synthesis rate of the reporter protein, γ_g [$\min^{-1}$] its degradation constant, and $\mu(t)$ [$\min^{-1}$] the growth rate. In the absence of post-transcriptional regulation, $p(t)$ varies with the rate of transcription of the reporter gene, and is therefore often called promoter activity (Ronen et al., 2002). In the case of transcriptional fusions, the promoter activity of the reporter is a good indicator of the promoter activity of the host gene. We recall that $\ln 2/\gamma_g$ equals the half-life of the reporter protein.

Given that the fluorescence is a measure of the quantity of GFP and the absorbance a measure of the total cell volume, we infer that

$$x_g(t) = \delta \frac{f(t)}{a(t)} \tag{S4}$$

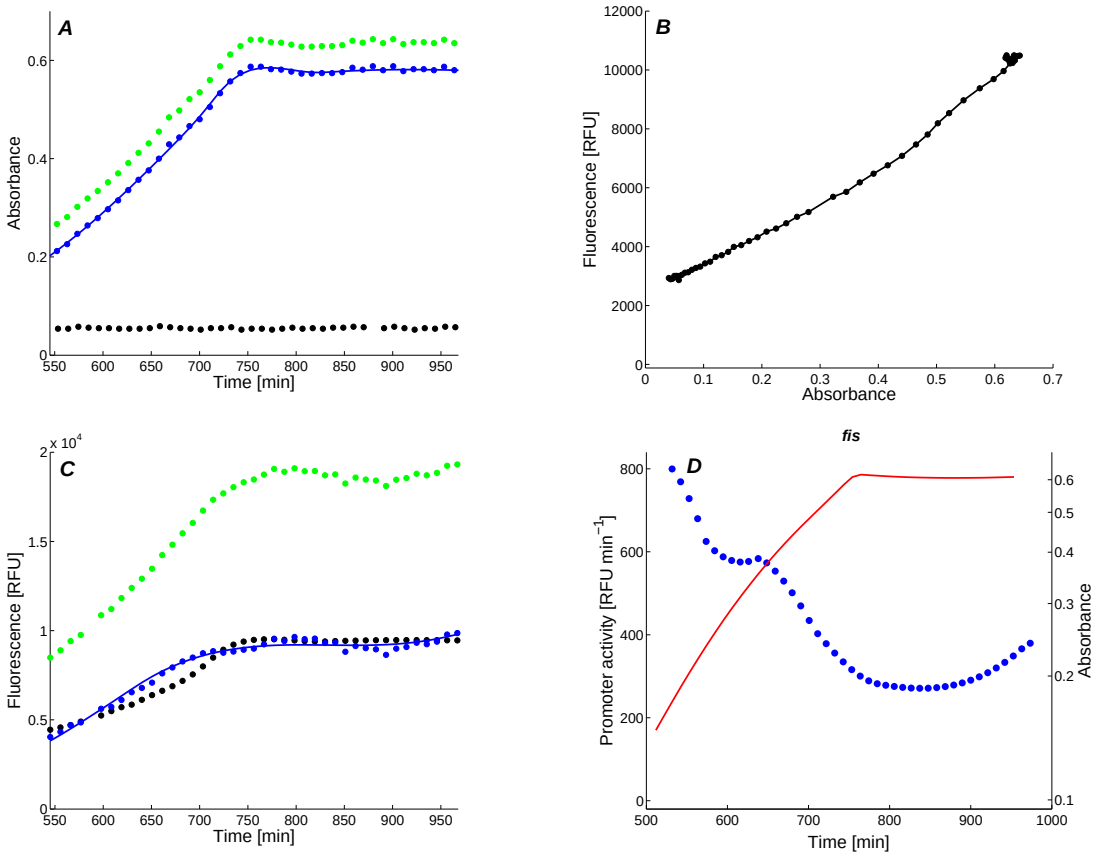

Figure S1: Example of the analysis of fluorescence reporter gene data. *A:* Primary (uncorrected) absorbance (•, green), background absorbance (•, black), and corrected absorbance (•, blue) for a wild-type strain with a pZE*fis-gfp* plasmid. The plot also shows the spline fit of the corrected data. *B:* Calibration curve for background correction obtained by means of the strain carrying the promoterless vector pZE*gfp*. Primary fluorescence data are plotted against corrected absorbance data. The curve is obtained by interpolation of the data points. *C:* Primary fluorescence (•, green) data for the pZE*fis-gfp* strain. The plot also shows the background fluorescence (•, black), and the corrected fluorescence obtained after subtracting the two with Eq. S2 (•, blue). *D:* Promoter activity of *fis* (•, blue) computed from the corrected absorbance (–, red) and fluorescence data by means of Eq. S6. Fig. 3*C* in the main text shows the mean and confidence intervals computed from 4 experimental replicates.

for some positive scaling constant δ [μM RFU^{-1}]. The growth rate is defined in terms of the absorbance, that is,

$$\mu(t) = \frac{da(t)}{dt}\frac{1}{a(t)} = \frac{d\ln(a(t))}{dt}. \tag{S5}$$

This allows Eq. S3 to be recast, after some basic calculus (de Jong et al., 2010), into an expression defining the promoter activity in terms of the measured fluorescence and absorbance intensities

$$p(t) = \delta\left(\frac{df(t)}{dt}\frac{1}{a(t)} + \gamma_g\frac{f(t)}{a(t)}\right). \tag{S6}$$

For $\mu(t) \gg \gamma_g$, the second term in the right-hand side of Eq. S6 can be neglected, and we obtain the expression for the promoter activity usually found in the literature (*e.g.*, Ronen et al. (2002)).

In the absence of knowledge of the value of δ, we arbitrarily set this parameter to 1, and thus express the promoter activity and reporter protein concentration in units RFU and RFU min^{-1}, respectively. This leads to a relative, instead of absolute measure of gene expression, which is usual for this kind of experiments and sufficient for our purpose. Recent developments in single-molecule measurements of gene expression will make absolute measurements of gene expression feasible in the future (Cai et al., 2006; Itzkovitz and van Oudenaarden, 2011).

In order to compute $p(t)$, the corrected absorbance and fluorescence data are fitted using cubic regression splines (de Jong et al., 2010). For the GFPmut3 reporter used in this study, $\gamma_g = 0.012 \pm 0.001$ min^{-1}, which corresponds to a half-life of about 1 h (de Jong et al., 2010). The GFPmut2 reporter has a much longer half-life of 16 h ($\gamma_g = 0.0007 \pm 0.0001$). We also take into account the maturation time of GFP (25 min for GFPmut3 and 4 min for GFPmut2), as explained in detail elsewhere (de Jong et al., 2010).

The promoter activities reported in the main text and in the Supporting Information are the mean of 3-4 experimental replicates. Replicates from wells on the edge of the microplate were eliminated if they showed significantly different growth kinetics. In order to correct for small inoculation differences, the replicates are synchronized with respect to the absorbance curves. In particular, based on the observation of Isalan et al. (2008) that the absorbance derivative profile provides a robust signature of bacterial growth, we synchronize the promoter activities with respect to the time-points t^* at which $da(t)/dt = 0$. The confidence intervals are computed from the standard error of the mean. More precisely, the plots show confidence intervals consisting of ± 2 standard errors of the mean, which under the assumption of Gaussian distributions corresponds to 95% confidence.

Fig. S2 shows the time-varying growth rates computed by means of Eq. S5 from the absorbance data, for the four experimental conditions considered in this manuscript.

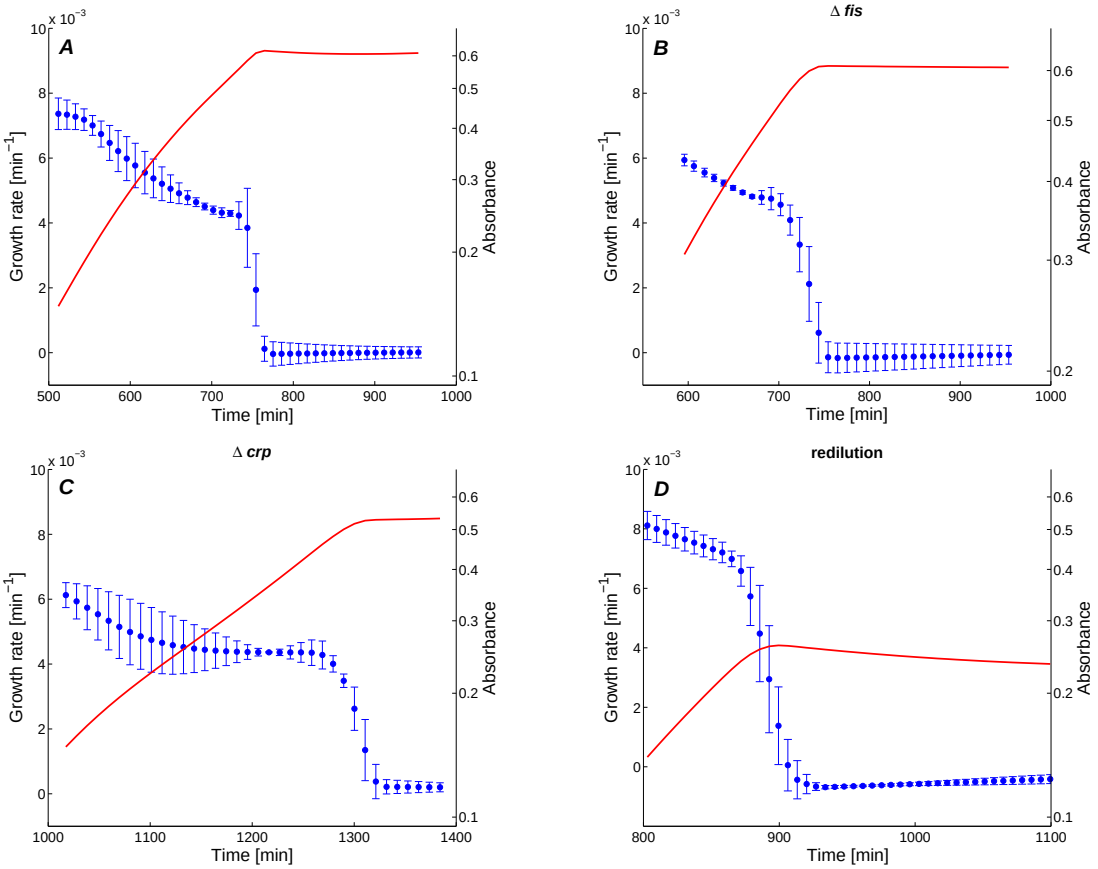

Figure S2: Growth rate computed from the corrected absorbance data by means of Eq. S5. The instantaneous growth-rate values are the mean of 4 replicates, synchronized with respect to the absorbance curves as described in Sec. S2. The confidence intervals are computed from the standard error of the mean. *A:* Wild-type strain with pZE*fis-gfp* plasmid. *B:* Idem for Δ*fis* strain. *C:* Idem for Δ*crp* strain. *D:* Idem for wild-type strain after redilution into low-glucose medium.

S3 Determination of intracellular cAMP concentration from experimental data

The concentration of cAMP (adenosine 3',5'-cyclic monophosphate) is measured by means of a commercially-available immunoassay kit (Upstate). The assay is a competitive ELISA where quantification occurs by a chemiluminescence signal originating from the competition for the

binding sites of a specific anti-cAMP antibody between extracellular cAMP contained in the sample and added, labeled cAMP. Following the manufacturer's instructions, the measured intensities are related to extracellular cAMP concentrations, that is, the concentration of cAMP exported from the cells into the growth medium by means of a calibration curve. For our purpose, we are interested in the cAMP concentration inside the cells, however, which is much more difficult to measure due to artifacts arising from cell collection and contamination with extracellular cAMP (Pastan and Adhya, 1976). We explain in this section how the intracellular cAMP concentration can be computed from the measured extracellular cAMP concentration.

The cAMP molecules in the medium are produced inside the cells and exported. Extracellular cAMP is not degraded and is a metabolic end-product (Epstein et al., 1975). Therefore, the accumulation of extracellular cAMP is the net sum of cAMP molecules exported from the cells and cAMP molecules imported back from the medium into the cells. Fig. S3 schematically summarizes the relation between intracellular and extracellular cAMP. The concentration of extracellular cAMP is obtained by dividing the molar quantity of cAMP in the sample by the volume of the sample. The concentration of intracellular cAMP is defined as the molar quantity of intracellular cAMP divided by the total volume of the cells in the sample. Whereas the sample volume is constant over the experiment, the total cell volume obviously changes over time.

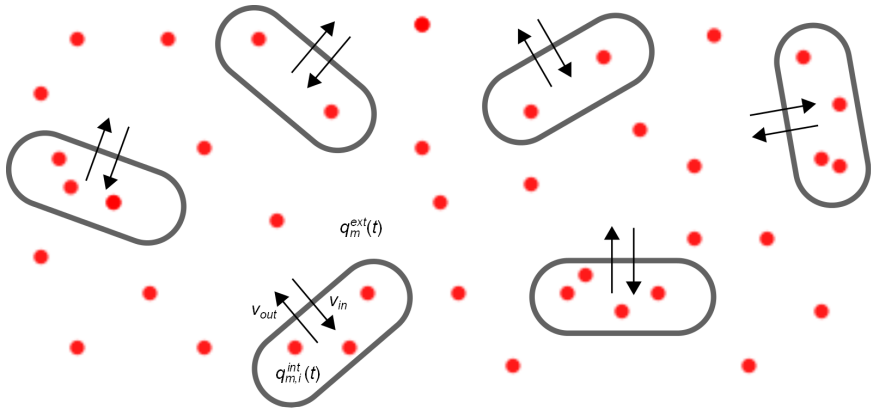

Figure S3: Relation between intracellular and extracellular cAMP in a bacterial culture. $n(t)$ is the number of cells at time t, $q_{m,i}^{int}(t)$ and $q_m^{ext}(t)$ are the quantities of cAMP inside cell i and in the growth medium, respectively, at time t. The rates v_{in} and v_{out} denote the transport into and from the cells. The red dots symbolize cAMP molecules.

In order to derive the concentration of cAMP inside the cells from the concentration of cAMP in the medium, we develop a simple kinetic model. We denote by $q_{m,i}^{int}(t)$ and $q_m^{ext}(t)$

the quantities of cAMP [mol] inside cell i and in the growth medium, respectively, at time t [min]. At time t there are $n(t) \geq 1$ cells in the sample, so $i \in \{1, \ldots, n(t)\}$. This gives the following balance equation for the quantity of external cAMP

$$\frac{dq_m^{ext}(t)}{dt} = \left[\sum_{i \in \{1,\ldots,n(t)\}} v_{out}(q_{m,i}^{int}(t)) \right] - n(t)\, v_{in}(q_m^{ext}(t)). \tag{S7}$$

The first term on the righthand side of Eq. S7 denotes the rate of export of cAMP from the cells into the growth medium, while the second term describes the rate of import of cAMP from the medium into the cells.

The export and import rates follow simple first-order kinetics (Epstein et al., 1975), so that v_{out} is a linear function of the internal cAMP concentrations with rate constant k_{out} [min^{-1}] and v_{in} a linear function of the external cAMP concentration with rate constant k_{in} [min^{-1}]. This yields

$$v_{out}(q_{m,i}^{int}(t)) = k_{out}\, q_{m,i}^{int}(t), \qquad v_{in}(q_m^{ext}(t)) = k_{in}\, q_m^{ext}(t). \tag{S8}$$

Defining

$$q_m^{int}(t) = \sum_{i \in \{1,\ldots,n(t)\}} q_{m,i}^{int}(t), \tag{S9}$$

we rewrite Eq. S7 as

$$\frac{dq_m^{ext}(t)}{dt} = k_{out}\, q_m^{int}(t) - n(t)\, k_{in}\, q_m^{ext}(t). \tag{S10}$$

In order to obtain concentration variables, we now introduce volume parameters V_{tot} and $V_{cell}(t)$, representing the sample volume [L] and the volume of individual cells [L], respectively. Notice that the cell volume is a function of time, since the growth rate changes over time and the cell volume varies with the growth rate (Bremer and Dennis, 1996; Volkmer and Heinemann, 2011). In order to obtain concentrations, the quantity of internal cAMP needs to be weighted by the total cellular volume, given by $n(t)\, V_{cell}(t)$, and the quantity of external cAMP by $V_{tot} - n(t)\, V_{cell}(t)$. Given that the cells occupy only a tiny fraction of the sample volume, the latter term is approximated by V_{tot}.

We multiply the left-hand and right-hand side of the equation with volume terms

$$\frac{dq_m^{ext}(t)}{dt}\, \frac{1}{V_{tot}} = k_{out}\, q_m^{int}(t)\, \frac{1}{V_{tot}}\, \frac{n(t)\, V_{cell}(t)}{n(t)\, V_{cell}(t)} - n(t)\, k_{in}\, \frac{1}{V_{tot}}\, q_m^{ext}(t),$$

which results in

$$\frac{du_m^{ext}(t)}{dt} = n(t)\, V_{cell}(t)\, \frac{k_{out}}{V_{tot}}\, u_m^{int}(t) - n(t)\, k_{in}\, u_m^{ext}(t). \tag{S11}$$

$u_m^{int}(t)$ and $u_m^{ext}(t)$ are the concentrations of intracellular and extracellular cAMP [M], respectively. From Eq. S11 we obtain the following expression for the concentration of intracellular cAMP:

$$u_m^{int}(t) = \frac{1}{n(t)\,V_{cell}(t)}\,\frac{V_{tot}}{k_{out}}\,\frac{du_m^{ext}(t)}{dt} + \frac{k_{in}}{k_{out}}\,\frac{V_{tot}}{V_{cell}(t)}\,u_m^{ext}(t). \tag{S12}$$

Using this equation, we can compute $u_m^{int}(t)$ from the measured concentration of extracellular cAMP. For this we need to know the constant k_{out}, the constant V_{tot}, the constant k_{in} and the total cellular volume $n(t)\,V_{cell}(t)$. k_{out} has been measured as 2.1 min^{-1} (Epstein et al., 1975), while the volume V_{tot} sampled from the wells equals 100 μL. Interestingly, Volkmer and Heinemann (2011) have shown that the ratio $n(t)\,V_{cell}(t)/a(t)$ is constant, where $a(t)$ is the measured absorbance of the culture volume in the microplate at time t. The value of this ratio, which we call α, can be computed for our conditions by means of a calibration curve previously obtained (de Jong et al., 2010), given that *E. coli* cells growing on glucose have a cell volume of about $3 \cdot 10^{-9}$ μL. We find $\alpha = 0.3$ μL and replace $n(t)\,V_{cell}(t)$ by $\alpha\,a(t)$. When equating the cell volume in the import term to $3 \cdot 10^{-9}$ μL, we obtain the expression

$$u_m^{int}(t) = \frac{1}{1.5 \cdot 10^{-3}\,a(t)\,k_{out}}\,\frac{du_m^{ext}(t)}{dt} + \frac{k_{in}}{3 \cdot 10^{-11}\,k_{out}}\,u_m^{ext}(t). \tag{S13}$$

The concentrations of extracellular cAMP and the absorbance were measured at different time-points. In particular, we took samples from a growing bacterial culture at 12 time-points. In order to obtain $u_m^{ext}(t)$ and $a(t)$, we fit a cubic regression spline to the data, and take the derivative of the u_m^{ext}-spline to obtain $du_m^{ext}(t)/dt$. The value of k_{in} can then be estimated from Eq. S13 by using the measured steady-state concentration for intracellular cAMP during exponential growth on glucose, namely 0.4 μM (Epstein et al., 1975; Pastan and Adhya, 1976), as well as the absorbance and the (time-derivative of the) extracellular cAMP concentration measured in our experiments. We thus find a value $k_{in} = 12 \cdot 10^{-10}$ min^{-1}.

With all parameter values thus known, Eq. S13 allows the reconstruction of the time-varying concentration of intracellular cAMP from the measured profiles of $a(t)$, $u_m^{ext}(t)$, and $du_m^{ext}(t)/dt$. One of the advantages of the use of splines is that the intracellular cAMP concentration can easily be calculated at all time-points by spline interpolation. The values for $u_m^{int}(t)$ reported in this manuscript are the mean of three replicates. The confidence intervals are computed from the standard error of the mean after synchronization of the absorbance curves, as described in Sec. S2.

Fig. S4*A*-*B* shows plots of the measured extracellular and derived intracellular cAMP concentrations for the wild-type strain in the reference conditions described in the Materials and methods section of the main text (M9 minimal medium with 0.3% glucose). The shape of

the intracellular cAMP concentration profile agrees very well with other, direct measurements (Buettner et al., 1973; Kao et al., 2004; Makman and Sutherland, 1965). cAMP rapidly accumulates at the end of exponential growth, when glucose is exhausted, and returns to a lower level after the growth transition. Panels *C* and *D* show the derived intracellular cAMP concentration profiles in two additional conditions (Δ*fis* strain and glucose down-shift). Although quantitative differences occur, we observe that the three intracellular cAMP profiles have the same qualitative shape.

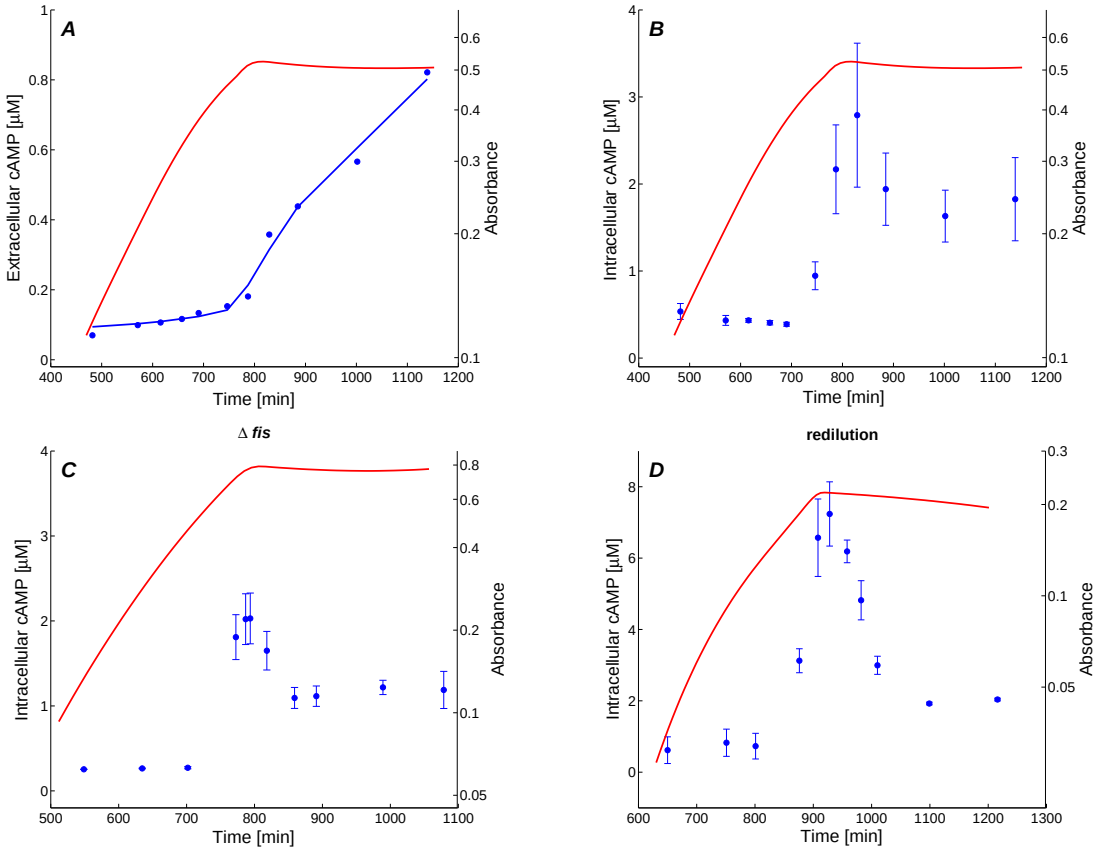

Figure S4: Measurements of cAMP concentration in samples taken from a bacterial culture growing in a microplate. *A:* Absorbance and measured concentration of extracellular cAMP, with spline fit to cAMP data. *B:* Absorbance and derived concentration of intracellular cAMP. The cAMP concentrations are the mean of 3 replicates, synchronized with respect to the absorbance curves as described in Sec. S2. The confidence intervals are computed from the standard error of the mean. This plot corresponds to Fig. 2*B* of the main text. *C:* Idem in Δ*fis* strain. *D:* Idem in wild-type strain after glucose down-shift.

S4 Comparison of constitutive promoters pRM and ptet

The pRM promoter of phage λ is regulated by the transcription factors CI and Cro (Oppenheim et al., 2005). Since the latter are not present in uninfected *E. coli* cells, the activity of pRM seems a good indicator of changes in the overall physiological state of the cell. Some phage promoters have co-evolved with regulatory factors in their host, and may thus not be genuinely constitutive (Slominska et al., 1999). Although there is no evidence in the literature that (p)ppGpp regulates pRM, and not all phage promoters are (p)ppGpp-dependent (Potrykus et al., 2002), we cannot exclude this hypothesis *a priori*.

We therefore compared the activity of pRM to that of another promoter believed to be constitutively expressed. If the time-varying activities of the two promoters agree well in our conditions, then it seems unlikely that pRM is controlled by an unknown regulatory factor (as such a factor would have to impact both promoters in the same way). As our control we chose the synthetic promoter pLtetO-1 or ptet (Lutz and Bujard, 1997), which is controlled by TetR, a transcription factor that is normally absent in *E. coli* cells. The ptet promoter has been used before as a prototypical constitutive promoter, for example by Klumpp et al. (2009).

Fig. S5*A*-*B* shows the time-varying promoter activities of pRM and ptet in the same experiment, under the reference conditions (wild-type bacteria growing in batch on M9 supplemented with 0.3% glucose). The profiles are virtually identical, with an approximately two-fold decrease of the promoter activities during the growth transition. The fusion of ptet with the fluorescent reporter gene is very strongly expressed, leading to a somewhat reduced growth rate in exponential phase and complicating a direct comparison of the activity profiles. In order to account for the difference in growth rate, following a commonly-used procedure (*e.g.*, Mangan et al. (2006)), we redefined time in terms of the number of generations before the growth arrest, and normalized the promoter activities with respect to the minimum reached after the transition. Fig. S5*C* shows that, when applying these corrections, the activity profiles of ptet and pRM are in excellent qualitative and quantitative agreement. We conclude that pRM indeed behaves as a constitutive promoter.

S5 Influence of cAMP on pRM activity

As a further control of the use of pRM as a constitutive promoter, we wanted to test if the expression of the pRM-*gfp* reporter was affected by cAMP. This hypothesis is *a priori* unlikely, as the promoter region does not contain any Crp·cAMP binding sites, but cannot be excluded. We experimentally tested cAMP-dependence by adding different concentrations

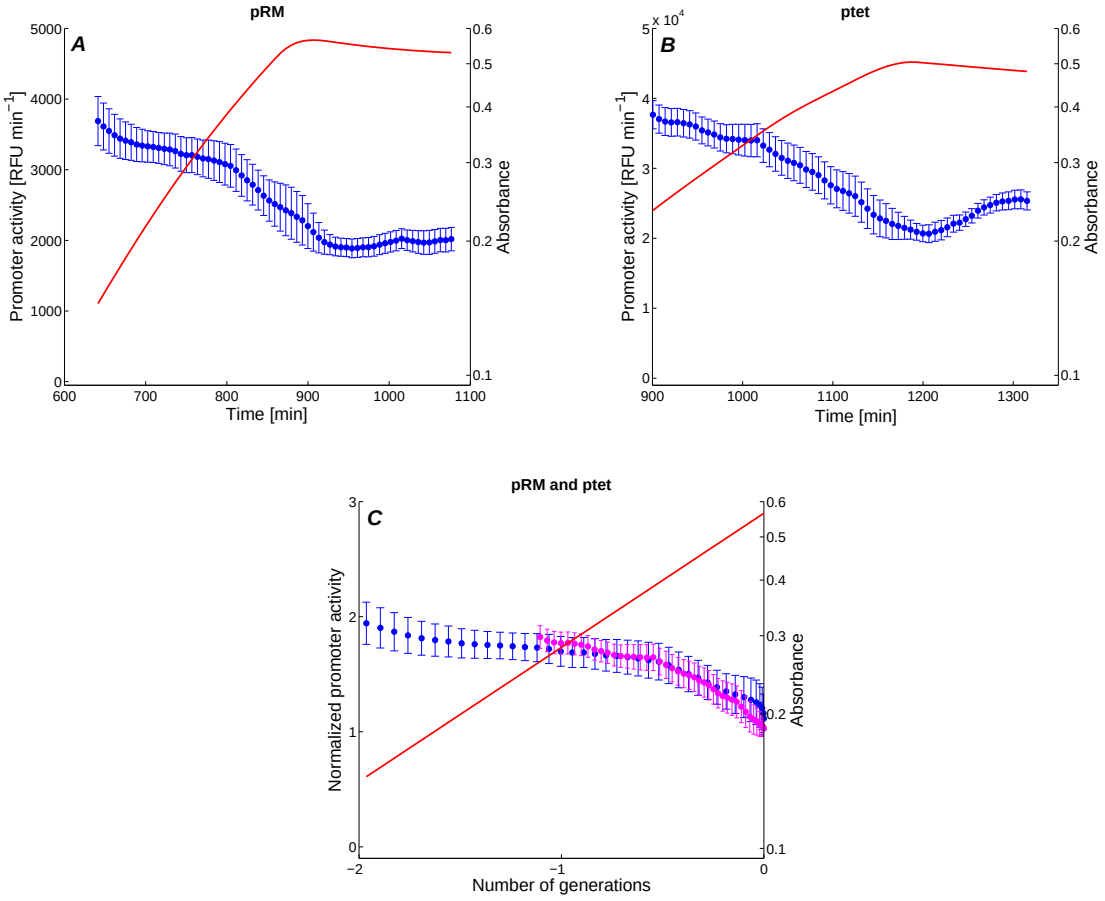

Figure S5: Experimental monitoring of activity of different constitutive promoters. *A:* Time-varying activity of the pRM promoter of phage λ (•, blue), derived from GFP data, and absorbance (solid line, red). *B:* Idem for the activity of ptet. *C:* Comparison of the activities of pRM (blue) and ptet (purple) after normalization and time rescaling. -1 corresponds to one generation before growth arrest. The data shown in the plots are the mean of 5 experimental replicates, with confidence intervals computed from the standard error of the mean.

of cAMP to the growth medium. Kuhlman et al. (2007) have shown that, in order to obtain sufficient variation in the concentration of intracellular cAMP, and thus differential expression of a Crp·cAMP-controlled gene, these experiments have to be carried out in a Δcya strain, incapable of endogenously producing cAMP. Moreover, the results shown in Fig. 1*B* of the same publication provide an indication of the appropriate range of variation of the external concentration of cAMP.

We transformed the Δcya strain of the Keio collection with the pZE1RM-*gfp* reporter plasmid (Sec. S1). We monitored the activity of the reporter gene in minimal medium supplemented with 0.3% glucose and different concentrations of external cAMP (100-2000 μM). We observed identical growth kinetics for the different cAMP concentrations, and we checked that the promoter activity of the gene *acs*, activated by Crp·cAMP, indeed increased when augmenting the external cAMP concentration. The results in Fig. S6 show that expression from the pRM promoter varies little over the range of cAMP concentrations applied. Overall, the data show that pRM transcription is not specifically regulated by cAMP.

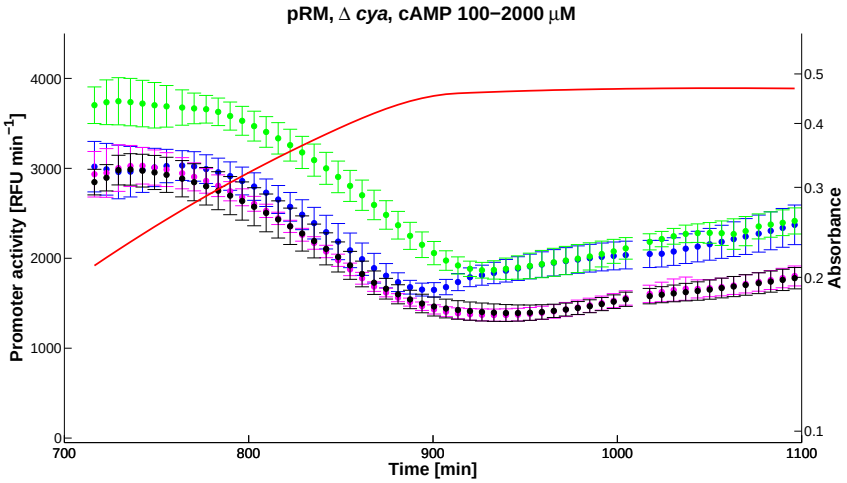

Figure S6: Experimental monitoring of activity of pRM promoter of phage λ in Δcya strain under various concentrations of externally-supplied cAMP. Time-varying activities of the pRM promoter of phage λ (•), derived from GFP data, and absorbance (solid line, red). The profiles are shown for 100 μM (black), 500 μM (purple), 1000 μM (green), and 2000 μM (blue). The data shown in the plots are the mean of 5 experimental replicates, with confidence intervals computed from the standard error of the mean.

S6 Measurement of time-varying plasmid copy number

We used quantitative PCR (qPCR) to determine the time-varying number of plasmids per chromosomal equivalent of DNA (plasmid copy number), following a previously validated protocol (Lee et al., 2004). We took 5 μL samples at 11 time-points from cultures of strains carrying a reporter plasmid, growing in a microplate under the conditions described in the Materials and methods section of the main text. The samples were diluted 20-100x into MESA Green qPCR Master Mix (Eurogentec), supplemented with primers for the plasmid β-lactamase gene (*bla*) and for the chromosomal d-1-deoxyxylulose 5-phosphate synthase gene (*dxs*). Quantitative PCR was performed in a StepOnePlus Real-Time PCR System (Applied Biosystems) according to the instructions of the manufacturer. Briefly, 20 μL reaction mixtures were incubated for 10 min at 95°C and 40 PCR cycles (15 s at 95°C, 10 s at 62°C and 10 s at 72°C). PCRs were run in quadruplicate. Raw data were transformed into threshold cycle (C_T) values. PCR amplification efficiencies for *bla* and *dxs* were determined by constructing standard curves from serial dilutions (Lee et al., 2004).

The results were analyzed by means of the following model for computing the relative plasmid copy number $r(t)$ at the sample time-points t, with respect to a reference time-point t^0 (Reiter et al., 2011):

$$r(t) = \frac{E_{bla}^{\Delta C_T^{bla}(t)}}{E_{dxs}^{\Delta C_T^{dxs}(t)}}, \tag{S14}$$

where C_T^{bla} and C_T^{dxs} are the C_T values for *bla* and *dxs*, respectively, $\Delta C_T^{bla}(t) = C_T^{bla}(t) - C_T^{bla}(t_0)$, $\Delta C_T^{dxs}(t) = C_T^{dxs}(t) - C_T^{dxs}(t_0)$, and t_0 is a reference time-point. As our reference, we chose a measurement during steady-state exponential growth on glucose. As a consequence, copy number changes are relative to the measured values in exponential phase. The efficiencies were measured to be nearly 100% for *dxs* ($E_{dxs} = 2$) and 91% for *bla* ($E_{dxs} = 1.91$).

The results obtained for the two vectors used in this study (the standard pZE*gfp* and the additional pUA66*gfp* plasmids) are shown in Fig. S7. The copy number of pZE*gfp* (used for monitoring the activity of the *crp*, *fis* and *rpoS* promoters as well as the constitutive promoters) changes by a factor of about 2. The copy number of pUA66*gfp* (used for *acs*) remains approximately constant. In Sec. S8 we discuss how the model of Eq. 1 in the main text can be straightforwardly refined to accommodate the use of vectors with different copy number variations.

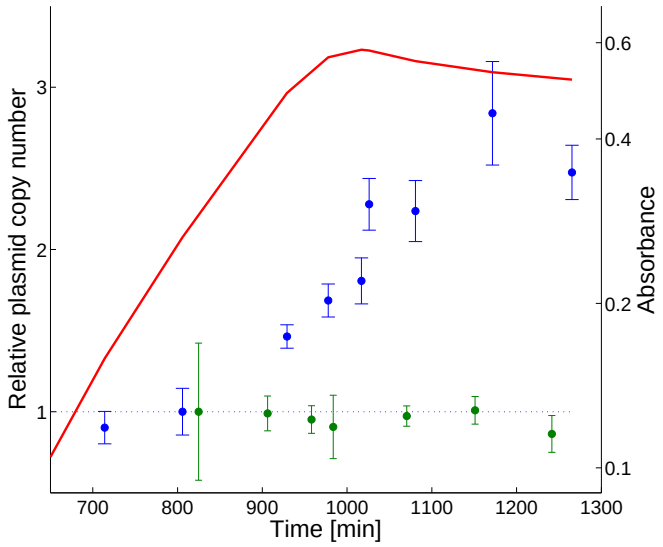

Figure S7: Variation of the number of plasmids per chromosomal equivalent of DNA (plasmid copy number) measured by means of qPCR. The quantities have been normalized with respect to the observed plasmid copy number in steady-state exponential growth on glucose. The confidence intervals were computed from the standard error of the mean of 4 replicates, after synchronization of the absorbance curves (Sec. S2). The plot shows the results for the pZE*gfp* (•, blue) and the pUA66*gfp* (•, green) vectors.

S7 Biological assumptions underlying promoter activity models: the case of Crp·cAMP-regulated genes

In this section, we explain the biological assumptions underlying the simple phenomenological models of promoter activity used in the main text, in particular for Crp·cAMP-regulated genes.

The essential feature of Eq. 1 is that, following previous work (*e.g.*, Klumpp et al. (2009); Kotte et al. (2010)), the terms for specific regulatory effects and the effect of the global physiological state enter the equation in a multiplicative way. In Eq. 3 the regulatory effect of Crp·cAMP is assumed to depend on the intracellular cAMP concentration ($p_2(t) = c(t)$). This simplification follows from the following assumptions:

1. The Crp concentration varies little in comparison with the cAMP concentration;
2. The basal promoter activity is much smaller than the maximal promoter activity;
3. The binding of cAMP to Crp is non-cooperative;
4. cAMP concentrations are not saturating.

The first assumption is justified from the experimental data (Fig. 2-3). Whereas during the transition the intracellular cAMP concentration changes at least 7-fold across the different conditions, the promoter activity of *crp* decreases only two-fold. Given a half-life on the order of hours, this means that the change in Crp concentration is negligible with respect to the change in cAMP concentration. Based on the first assumption, the following phenomenological model is used to describe the promoter activity of a Crp·cAMP-activated gene:

$$p(t) = p_1(t)\, b\, \frac{1 + f_c\,(c(t)/K_c)^n}{1 + (c(t)/K_c)^n}, \tag{S15}$$

where b [M min^{-1}] is a basal promoter activity, f_c the maximum fold-change after cAMP induction, n a Hill coefficient, and K_c [M] a half-saturation constant lumping the effects of the association/dissociation of Crp and cAMP and the association/dissociation of Crp·cAMP to the promoter. The model has been taken from (Kuhlman et al., 2007), and extended with the term $p_1(t)$, contained between 0 and 1, which represents the (normalized) effect of the global physiological state on the activity of the promoter (see Eq. 1 in the main text).

The second assumption implies that $1 \ll f_c\,(c(t)/K_c)^n$. As a consequence, Eq. S15 can be simplified to

$$p(t) = p_1(t)\, b\, f_c\, \frac{(c(t)/K_c)^n}{1 + (c(t)/K_c)^n}. \tag{S16}$$

This assumption is justified for *acs*, but probably not for all Crp·cAMP-regulated genes.

The third assumption amounts to the non-cooperative nature of the interaction between cAMP and Crp, in agreement with biochemical studies reviewed by Kuhlman and colleagues (Kuhlman et al. (2007) and references therein). It means that $n = 1$ and, as a consequence,

$$p(t) = p_1(t)\, b\, f_c\, \frac{c(t)/K_c}{1 + c(t)/K_c}. \tag{S17}$$

The fourth assumption states that $c(t)$ does not reach values that are much larger than K_c and that, as a consequence, the ratio $(c(t)/K_c)/(1 + (c(t)/K_c))$ varies in the linear range. This seems to be the case for the promoter activity of *acs*, which is seen to follow the accumulation of cAMP during the growth transition. Under the fourth assumption, Eq. S17 further simplifies to

$$p(t) = k\, p_1(t)\, c(t), \tag{S18}$$

with $k = b\, f_c/2K_c$. This equation straightforwardly leads to Eq. 4 of the main text.

S8 Effect of variation of plasmid copy number

The use of reporter genes has several advantages (ease of construction, signal strength), but may introduce a bias due to the variation of the plasmid copy number with the growth rate (Lin-Chao and Bremer, 1986). We show below that this bias does not affect the results of the analysis presented in the main text, based on Eqs. 2-3, if the promoter activities of the constitutive and target gene are monitored by means of the same plasmid vector. If this is not the case, the bias can easily be corrected using the qPCR data of Fig. S7.

In order to take into account the plasmid copy number variation, we make an explicit distinction between $p(t)$, the activity of a promoter on the chromosome, and $\hat{p}(t)$, the activity of the same promoter on a reporter plasmid. Let $r(t)$ denote the (time-varying) relative plasmid copy number, that is, the number of plasmids per chromosomal equivalent of DNA relative to a reference state at t_0 (Sec. S6). Then we have

$$\frac{\hat{p}(t)}{\hat{p}^0} = r(t)\, \frac{p(t)}{p^0}. \tag{S19}$$

In our reporter gene experiments we do not directly measure $p(t)$, but rather $\hat{p}(t)$. As a consequence, Eqs. 2-3 in the main text are redefined as

$$\log \frac{\hat{p}(t)}{\hat{p}^0} = \log \frac{\hat{p}_{RM}(t)}{\hat{p}^0_{RM}} \tag{S20}$$

$$\log \frac{\hat{p}(t)}{\hat{p}^0} - \log \frac{\hat{p}_{RM}(t)}{\hat{p}^0_{RM}} = \log \frac{c(t)}{c^0}. \tag{S21}$$

Substituting the expression for $p(t)/p^0$ into these equations yields

$$\log \left(r(t) \frac{p(t)}{p^0} \right) = \log \left(r_{RM}(t) \frac{p_{RM}(t)}{p^0_{RM}} \right)$$

$$\log \left(r(t) \frac{p(t)}{p^0} \right) - \log \left(r_{RM}(t) \frac{p_{RM}(t)}{p^0_{RM}} \right) = \log \frac{c(t)}{c^0},$$

We now distinguish between two different cases. First, the constitutive promoter (pRM) and the promoter of the target gene are carried by the same plasmid vector, as is the case for *crp*, *fis* and *rpoS* (Table S2). In this case, $r(t) = r_{RM}(t)$ and it is easy to see that, by eliminating the terms $r(t)$ and $r_{RM}(t)$, the original Eqs. 2-3 are obtained. That is, the variation of the plasmid copy number equally affects the terms $p(t)$ and $p_{RM}(t)$, and therefore cancels out.

Second, if the constitutive promoter (pRM) and the promoter of the target gene are carried on different plasmid vectors, as is the case for *acs* (Table S2), the terms $r(t)$ and $r_{RM}(t)$ do not cancel out. We obtain the following equations that contain a correction term for the difference in relative plasmid copy numbers:

$$\log \left(\frac{p(t)}{p^0} \right) = \log \left(\frac{p_{RM}(t)}{p^0_{RM}} \right) + \log \frac{r_{RM}(t)}{r(t)}, \tag{S22}$$

$$\log \left(\frac{p(t)}{p^0} \right) - \log \left(\frac{p_{RM}(t)}{p^0_{RM}} \right) = \log \frac{c(t)}{c^0} + \log \frac{r_{RM}(t)}{r(t)}, \tag{S23}$$

The time-varying ratio $r_{RM}(t)/r(t)$ has been measured in this work. It corresponds to the ratio of the measured relative copy numbers of the pZE*gfp* (blue) and pUA66*gfp* (black) vectors in Fig. S7. The data points have been fitted with a regression spline, and the computed ratio has been used to refine the model for *acs*. The confrontation of this refined model with the experimental data is shown in Fig. 4*C-D* of the main text.

Overall, the effect of the correction is modest, as can be verified in Fig. S8 below, which compares the models with and without bias correction. The calculated coefficients of determination do not vary much either. For instance, for the models taking into account the regulatory effect of cAMP (panels *C-D*), R^2 increases from 0.74 to 0.93.

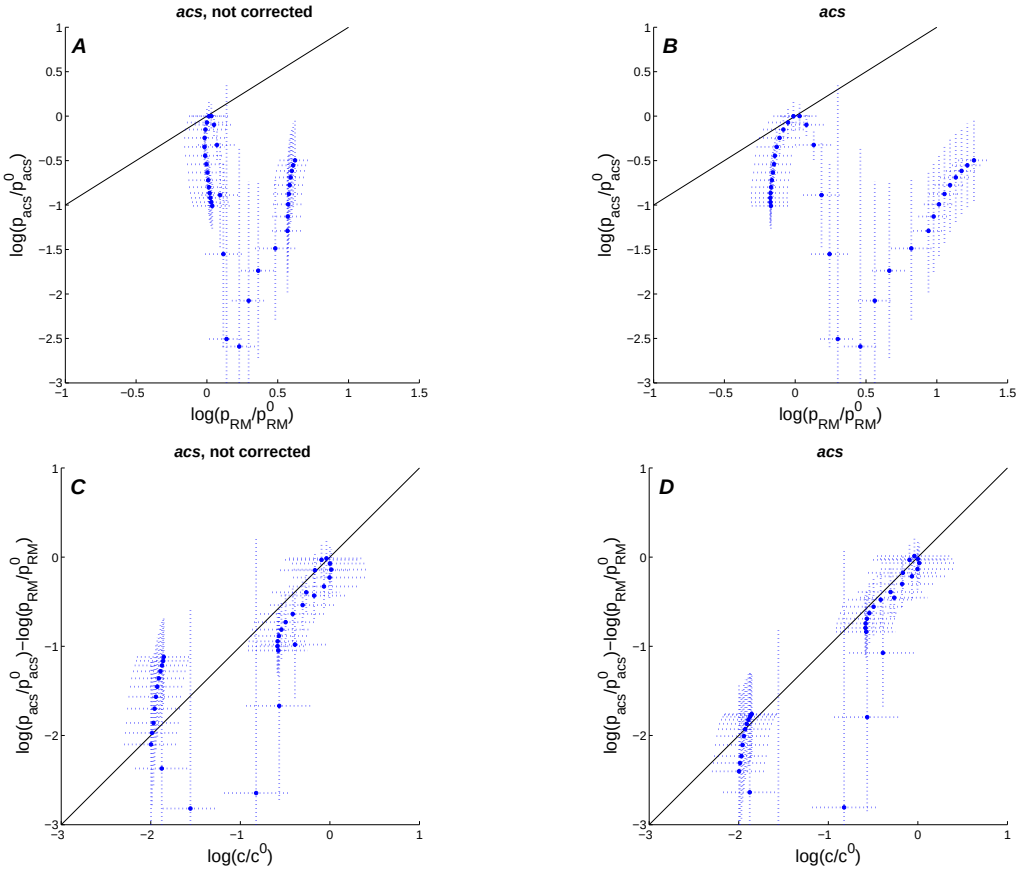

Figure S8: Predicted and observed control of *acs* activity using models with and without correction for the bias introduced by the use of different plasmid vectors. *A:* Predicted (–, black) and measured (•, blue) relative activity of the *acs* promoter ($\log(p_{acs}(t)/p^0_{acs})$) as a function of the relative activity of the pRM promoter ($\log(p_{RM}(t)/p^0_{RM})$). *B:* Idem, but including an additional correction factor for plasmid copy number bias ($\log(p_{RM}(t)/p^0_{RM}) + \log(r_{RM}(t)/r_{acs}(t))$). *C:* Predicted (–, black) and measured (•, blue) remaining relative activity of the *acs* promoter after subtraction of the effect of global physiological parameters ($\log(p_{acs}(t)/p^0_{acs}) - \log(p_{RM}(t)/p^0_{RM})$) and as a function of the relative intracellular cAMP concentration ($\log(c(t)/c^0)$). *D:* Idem, but including an additional correction factor for plasmid copy number bias ($\log(c(t)/c^0) + \log(r_{RM}(t)/r_{acs}(t))$). The panels *B* and *D* correspond to Fig. 4*C* and *D* in the main text, respectively.

S9 Additional gene expression profiles

Fig. 3 in the main text shows the gene expression response of the network, for the *fis*, *crp*, *acs*, *rpoS*, and pRM promoters in the reference conditions (depletion of glucose by wild-type bacteria in batch culture), as well as for the *acs* promoter in the case of Δ*fis* and Δ*crp* mutants. The figures in this section show additional data referred to in the manuscript.

Fig. S9 shows the primary fluorescence and absorbance data that were used to derive the activities of the *fis*, *crp* and *acs* promoters as well as the activity of the pRM promoter of phage λ in the reference conditions (reported in Fig. 3 in main text), according to the method outlined in Sec. S2. The plots in Fig. S9 show the data for a single well of the microplate.

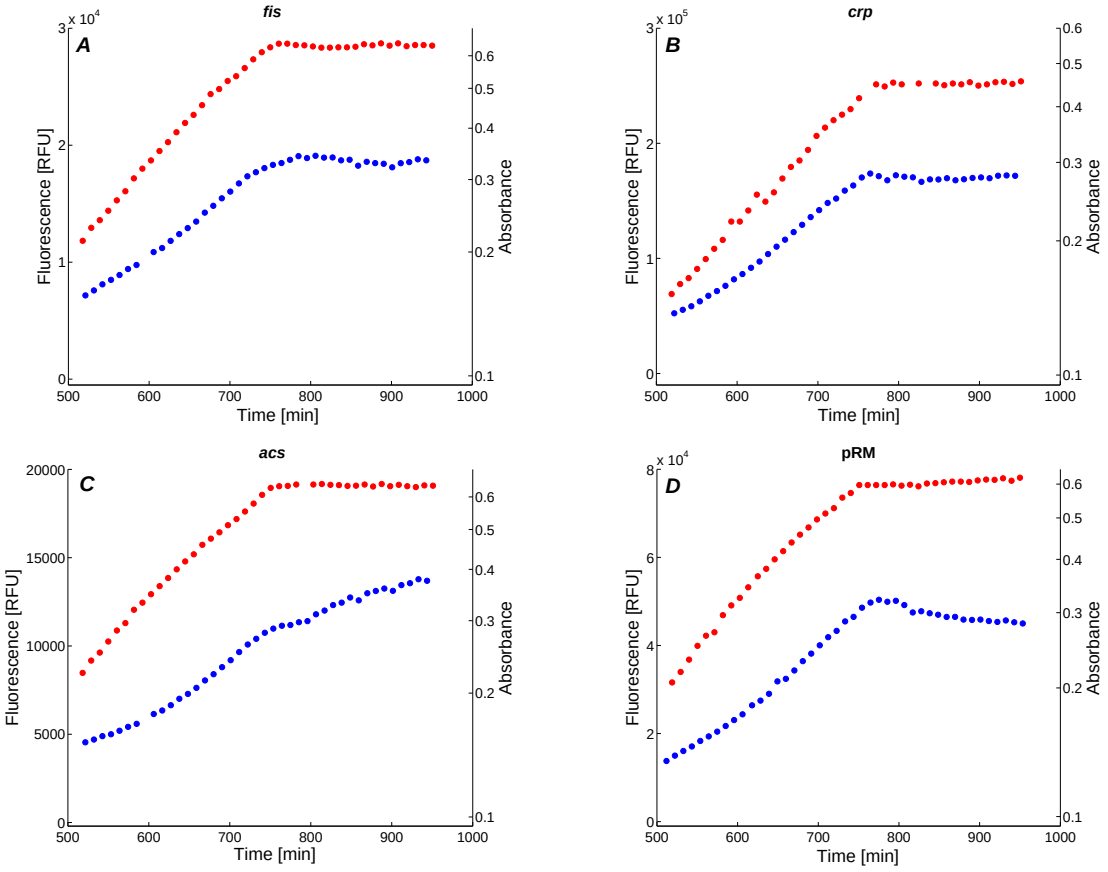

Figure S9: Primary data for computation of promoter activities. *A:* Primary (uncorrected) absorbance (•, red) and fluorescence (•, blue) data for the pZE*fis-gfp* strain. *B-D:* Idem for data from pZE*crp-gfp*, pUA66*acs-gfp*, and pZE1RM*gfp*. The primary data in this figure have been used to derive the promoter activities shown in Fig. 3 of the main text.

Fig. S10 shows the activities of the *fis*, *crp* and *acs* promoters as well as the activity of

the pRM promoter in a Δ*fis* mutant. Idem Fig. S11 and Fig. S12 for a Δ*crp* mutant and a wild-type strain after redilution into a low-glucose medium, respectively.

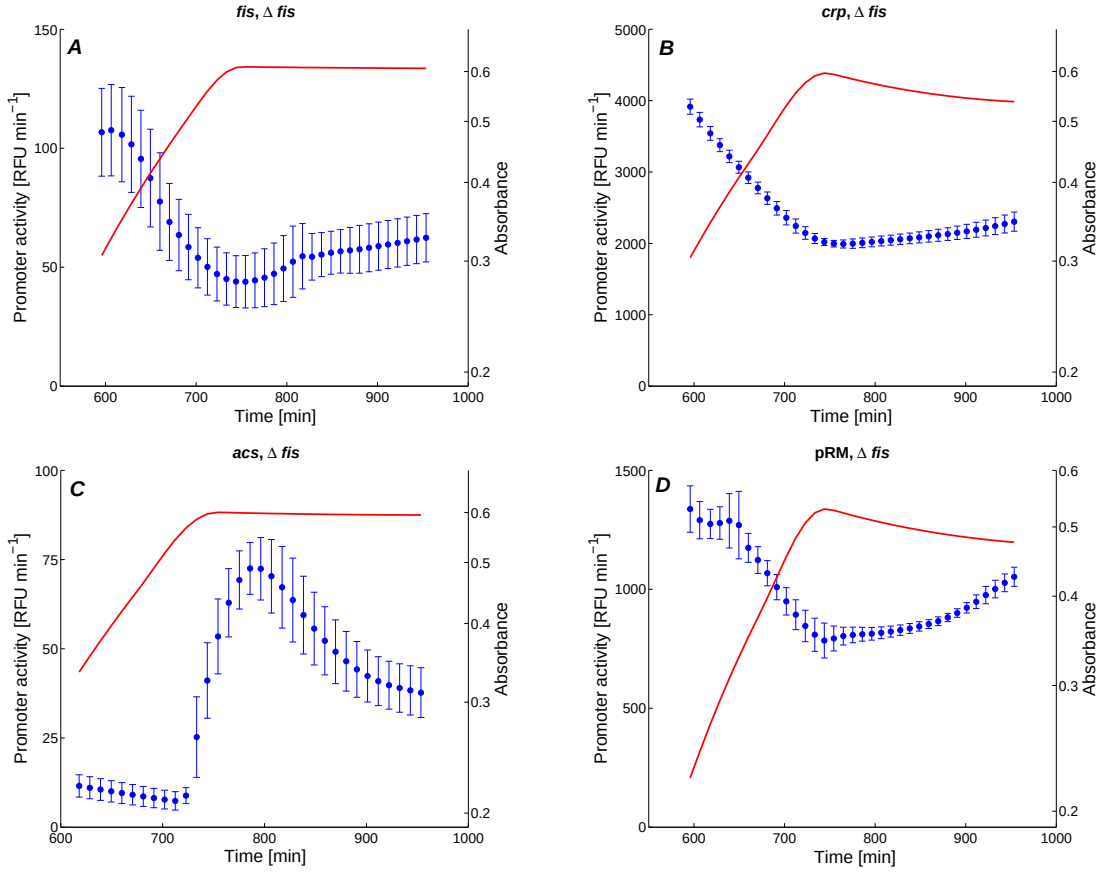

Figure S10: Experimental monitoring of promoter activities in Δ*fis* strain. *A:* Time-varying activity of *fis* promoter (•, blue), derived from GFP data, and absorbance (solid line, red). *B-D:* Idem for activities of *crp* and *acs* promoters as well as pRM promoter of phage λ. Panel C corresponds to Fig. 3*F* of the main text.

Fig. S13 shows the activity of the *rpoS* promoter, coding for the master stress regulator RpoS (σ^S), in the four conditions considered in this manuscript (wild-type, Δ*fis*, Δ*crp*, and redilution into low-glucose medium).

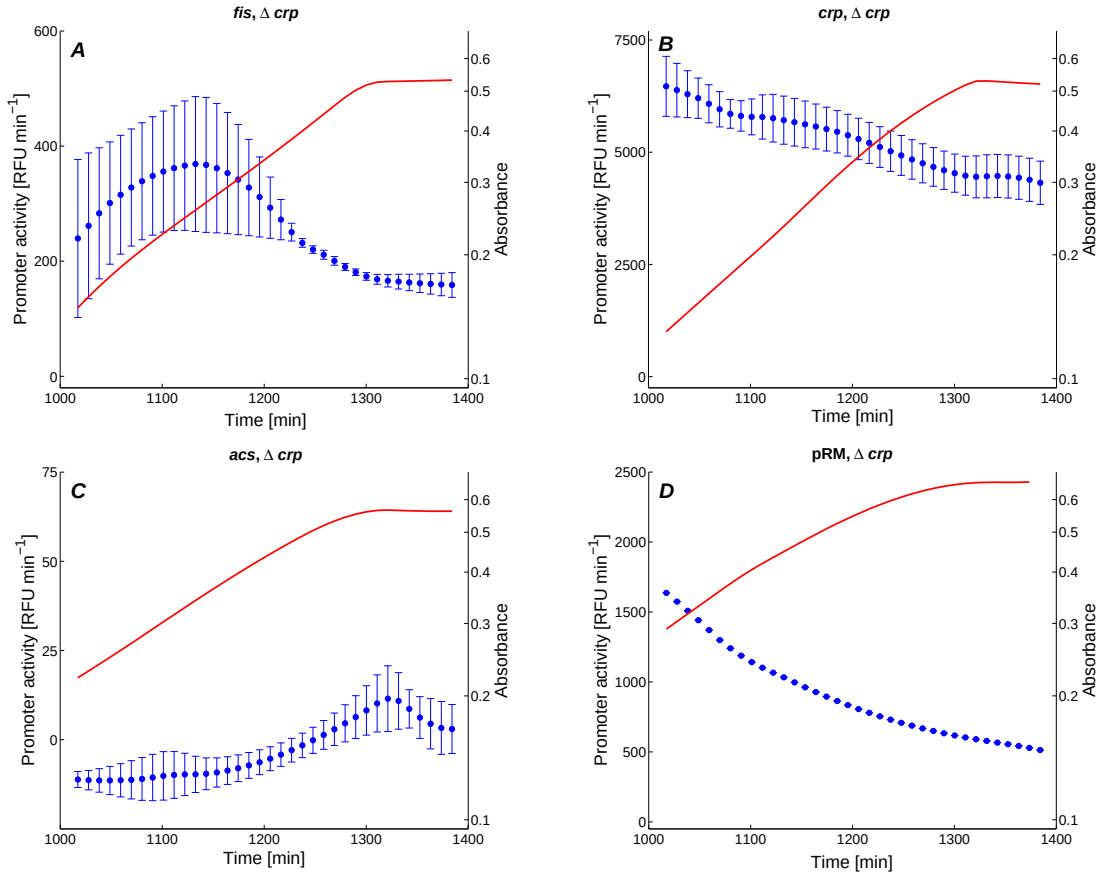

Figure S11: Experimental monitoring of promoter activities in Δcrp strain. *A:* Time-varying activity of *fis* promoter (•, blue), derived from GFP data, and absorbance (solid line, red). *B-D:* Idem for activities of *crp* and *acs* promoters as well as pRM promoter of phage λ.

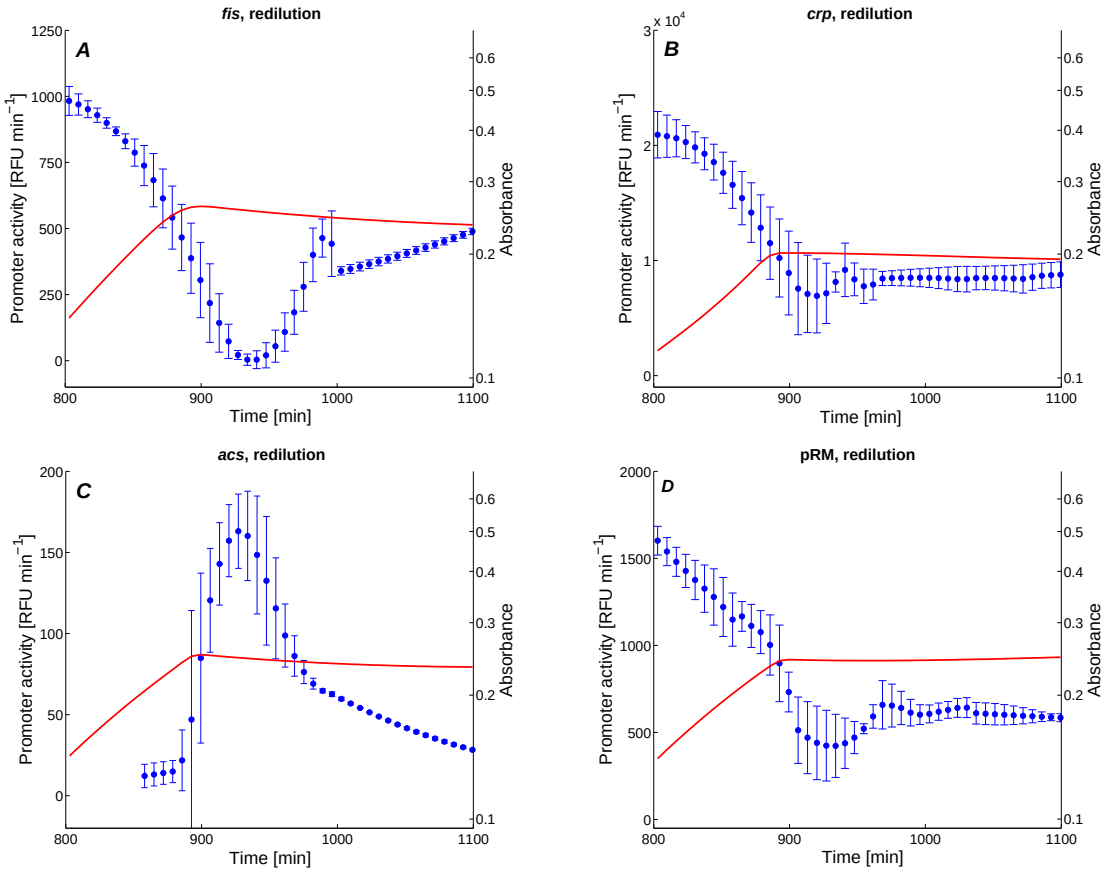

Figure S12: Experimental monitoring of promoter activities in wild-type strain after redilution into low-glucose medium. *A:* Time-varying activity of *fis* promoter (•, blue), derived from GFP data, and absorbance (solid line, red). *B-D:* Idem for activities of *crp* and *acs* promoters as well as pRM promoter of phage λ.

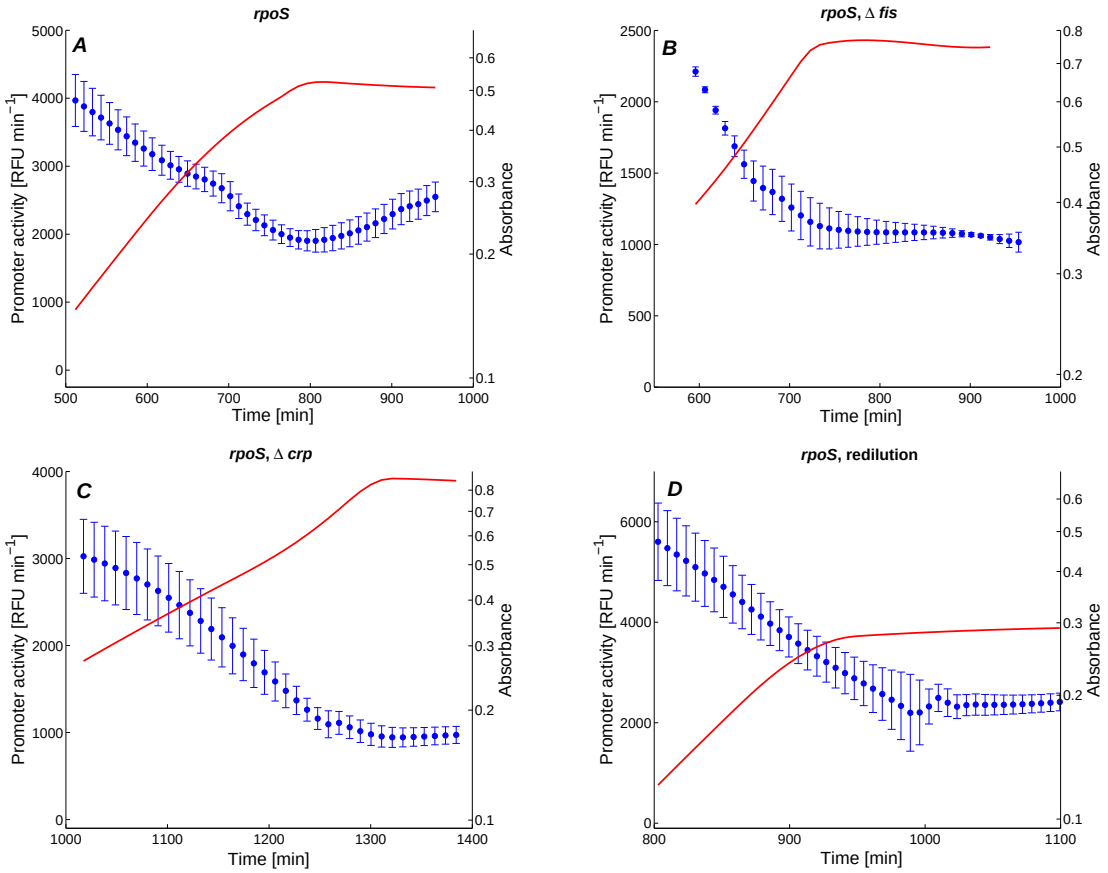

Figure S13: Experimental monitoring of the promoter activity of *rpoS*. *A:* Time-varying activity of *rpoS* promoter (•, blue), derived from GFP data, and absorbance (solid line, red). This plot corresponds to Fig. 3*D* in the main text. *B:* Idem for Δ*fis* mutant. *C:* Idem for Δ*crp* mutant. *D:* Idem for wild-type strain rediluted into low-glucose medium.

Experimental condition	Model	Equation	R^2
Wild-type	p_{fis} vs p_{RM}	Eq. 3	0.93
	p_{crp} vs p_{RM}	Eq. 3	0.96
	p_{acs} vs p_{RM}	Eq. 3	0.08
	p_{rpoS} vs p_{RM}	Eq. 3	0.84
	$p_{fis} - p_{RM}$ vs cAMP	Eq. 4	0.03
	$p_{crp} - p_{RM}$ vs cAMP	Eq. 4	0.02
	$p_{acs} - p_{RM}$ vs cAMP	Eq. 4	0.93
	$p_{rpoS} - p_{RM}$ vs cAMP	Eq. 4	0.54
Δfis	p_{fis} vs p_{RM}	Eq. 3	0.70
	p_{crp} vs p_{RM}	Eq. 3	0.92
	p_{acs} vs p_{RM}	Eq. 3	0.59
	p_{rpoS} vs p_{RM}	Eq. 3	0.88
	$p_{acs} - p_{RM}$ vs cAMP	Eq. 4	0.96
Δcrp	p_{fis} vs p_{RM}	Eq. 3	0.94
	p_{crp} vs p_{RM}	Eq. 3	0.96
	p_{rpoS} vs p_{RM}	Eq. 3	0.96
Wild-type and redilution	p_{fis} vs p_{RM}	Eq. 3	0.88
	p_{crp} vs p_{RM}	Eq. 3	0.96
	p_{acs} vs p_{RM}	Eq. 3	0.15
	p_{rpoS} vs p_{RM}	Eq. 3	0.86
	$p_{fis} - p_{RM}$ vs cAMP	Eq. 4	0.22
	$p_{crp} - p_{RM}$ vs cAMP	Eq. 4	< 0.01
	$p_{acs} - p_{RM}$ vs cAMP	Eq. 4	0.63
	$p_{rpoS} - p_{RM}$ vs cAMP	Eq. 4	0.40

Table S4: Summary of the coefficients of determination (R^2) for the models of Eq. 3-4 in the main text, for different genes and in different experimental conditions. For each model, we give the equation and an informal description summarizing the factors taken into account.

S10 Additional experimental tests of the models

The plots in Fig. 4 of the main text show the relative contributions of the global physiological state and specific transcription regulators to the control of the promoter activities of the genes considered in this study. Fig. S14 shows additional data referred to in the manuscript.

Table S4 summarizes the coefficients of determination obtained by the different models for all genes of the network under the different experimental conditions. The coefficient of determination, the square of the correlation coefficient, quantifies the fit of the model with the experimental data. In order to compute the correlation coefficient, the data points have been weighted by the inverse square of the confidence interval, thus giving more weight to precise values.

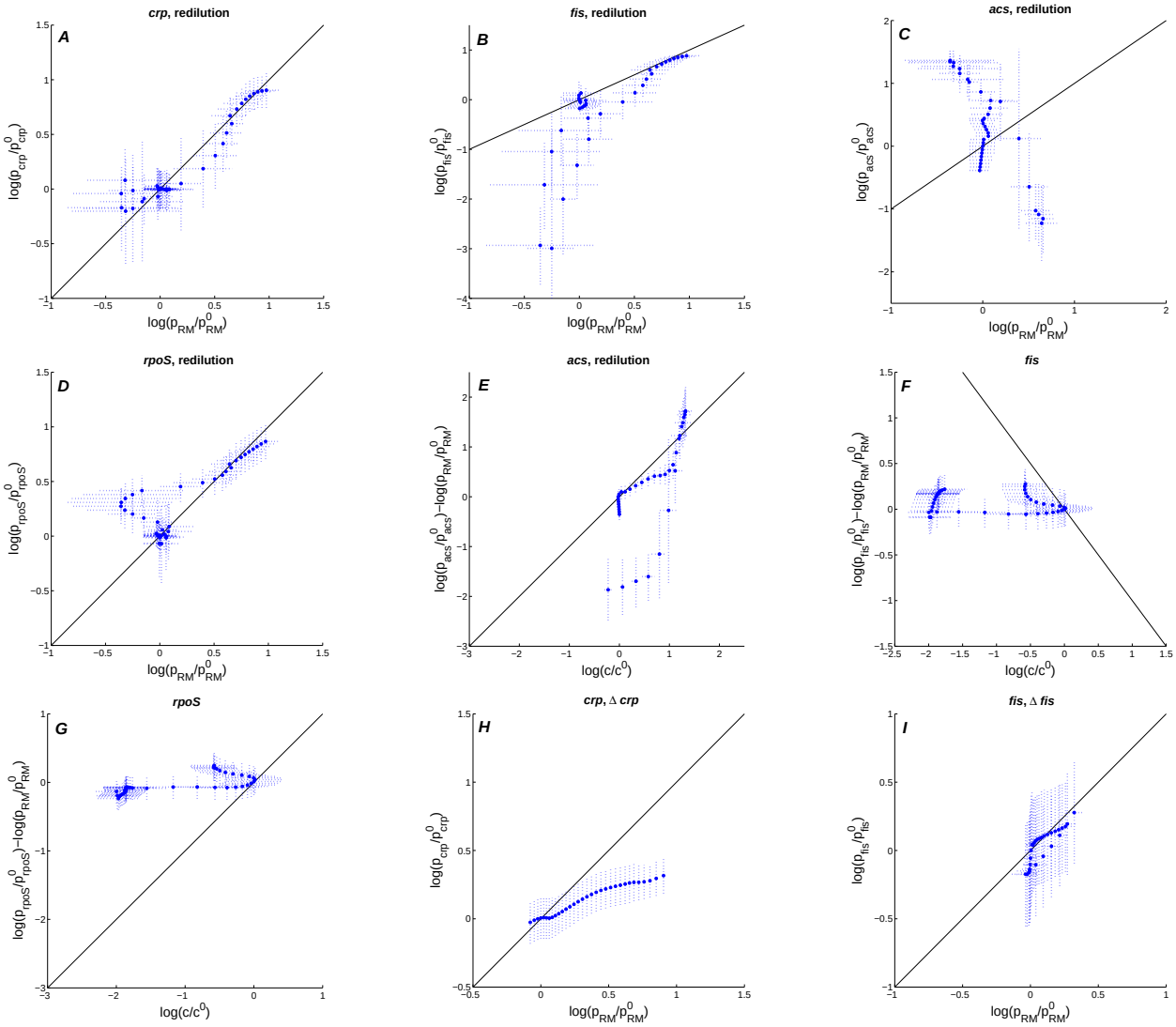

Figure S14: Predicted and observed control of *rpoS*, *fis*, *crp*, and *acs* activity by Crp·cAMP and the global physiological state, in various experimental conditions and genetic backgrounds. *A:* Predicted (–, black) and measured (•, blue) relative activity of the *crp* promoter ($\log(p_{crp}(t)/p^0_{crp})$) as a function of the relative activity of the pRM promoter ($\log(p_{RM}(t)/p^0_{RM})$) in a wild-type strain after a down-shift into a low-glucose medium. The confidence intervals in the plots have been computed from experimental replicas, as described in Sec. S2. *B-D:* Idem for *fis*, *acs*, and *rpoS* promoters. *E:* Predicted (–, black) and measured (•, blue) remaining relative activity of the *acs* promoter after subtraction of the effect of global physiological parameters ($\log(p_{acs}(t)/p^0_{acs}) - \log(p_{RM}(t)/p^0_{RM})$) and as a function of the relative intracellular cAMP concentration ($\log(c(t)/c^0)$). The experiments have been carried out with a wild-type strain after a down-shift into a low-glucose medium. *F:* Predicted (–, black) and measured (•, blue) remaining relative activity of the *fis* promoter after subtraction of the effect of global physiological parameters ($\log(p_{fis}(t)/p^0_{fis}) - \log(p_{RM}(t)/p^0_{RM})$) and as a function of the relative intracellular cAMP concentration ($\log(c(t)/c^0)$). *G:* Idem, but for *rpoS* promoter. *H:* Predicted (–, black) and measured (•, blue) relative activity of the *crp* promoter ($\log(p_{crp}(t)/p^0_{crp})$) as a function of the relative activity of the pRM promoter ($\log(p_{RM}(t)/p^0_{RM})$) in a Δ*crp* strain. *I:* Idem for *fis* promoter in a Δ*fis* strain.

References

T. Baba, T. Ara, M. Hasegawa, Y. Takai, Y. Okumura, M. Baba, K.A. Datsenko, M. Tomita, B.L. Wanner, and H. Mori. Construction of *Escherichia coli* K-12 in-frame, single-gene knockout mutants: the Keio collection. *Mol. Syst. Biol.*, 2:2006.0008, 2006.

F. Boyer, B. Besson, G. Baptist, J. Izard, C. Pinel, D. Ropers, J. Geiselmann, and H. de Jong. WellReader: a MATLAB program for the analysis of fluorescence and luminescence reporter gene data. *Bioinformatics*, 26(9):1262–63, 2010.

H. Bremer and P.P. Dennis. Modulation of chemical composition and other parameters of the cell by growth rate. In F.C. Neidhardt, R. Curtiss III, J.L. Ingraham, E.C.C. Lin, K.B. Low, B. Magasanik, W.S. Reznikoff, M. Riley, M. Schaechter, and H.E. Umbarger, editors, *Escherichia coli and Salmonella: Cellular and Molecular Biology*, pages 1553–69. ASM Press, Washington, DC, 2nd edition, 1996.

M.J. Buettner, E. Spitz, and H.V. Rickenberg. Cyclic adenosine 3',5'-monophosphate in *Escherichia coli*. *J. Bacteriol.*, 14(3):1068–73, 1973.

L. Cai, N. Friedman, and X.S. Xie. Stochastic protein expression in individual cells at the single molecule level. *Nature*, 440(7082):358–62, 2006.

H. de Jong, C. Ranquet, D. Ropers, C. Pinel, and J. Geiselmann. Experimental and computational validation of models of fluorescent and luminescent reporter genes in bacteria. *BMC Syst. Biol.*, 4:55, 2010.

M.B. Elowitz and S. Leibler. A synthetic oscillatory network of transcriptional regulators. *Nature*, 403(6767):335–8, 2000.

W. Epstein, L.B. Rothman-Denes, and J. Hesse. Adenosine 3':5'-cyclic monophosphate as mediator of catabolite repression in *Escherichia coli*. *Proc. Nat. Acad. Sci. USA*, 72(6): 2300–4, 1975.

D.G. Gibson. Enzymatic assembly of overlapping DNA fragments. *Methods Enzymol.*, 498: 349–61, 2011.

M. Isalan, C. Lemerle, K. Michalodimitrakis, C. Horn, P. Beltrao, E. Raineri, M. Garriga-Canut, and L. Serrano. Evolvability and hierarchy in rewired bacterial gene networks. *Nature*, 452(7189):840–5, 2008.

S. Itzkovitz and A. van Oudenaarden. Validating transcripts with probes and imaging technology. *Nat. Methods*, 8(4 Supp):S12–9, 2011.

K.C. Kao, Y.-L. Yang, R. Boscolo, C. Sabatti, V. Roychowdhury, and J.C. Liao. Transcriptome-based determination of multiple transcription regulator activities in *Escherichia coli* by using network component analysis. *Proc. Natl. Acad. Sci. USA*, 101 (2):641–6, 2004.

S. Klumpp, Z. Zhang, and T. Hwa. Growth rate-dependent global effects on gene expression in bacteria. *Cell*, 139(7):1366–75, 2009.

O. Kotte, J.B. Zaugg, and M. Heinemann. Bacterial adaptation through distributed sensing of metabolic fluxes. *Mol. Syst. Biol.*, 6:355, 2010.

T. Kuhlman, Z. Zhang, M.H. Saier Jr., and T. Hwa. Combinatorial transcriptional control of the lactose operon of *Escherichia coli*. *Proc. Nat. Acad. Sci. USA*, 104(14):6043–8, 2007.

C. Lee, J. Kim, S.G. Shin, and S. Hwang. Absolute and relative QPCR quantification of plasmid copy number in *Escherichia coli*. *J. Biotechnol.*, 123(3):273–80, 2004.

S. Lin-Chao and H. Bremer. Effect of the bacterial growth rate on replication control of plasmid pBR322 in *Escherichia coli*. *Mol. Gen. Genet.*, 203(1):143–9, 1986.

R. Lutz and H. Bujard. Independent and tight regulation of transcriptional units in *Escherichia coli* via the LacR/O, the TetR/O and AraC/I_1-I_2 regulatory elements. *Nucleic Acids Res.*, 25(6):1203–10, 1997.

R.S. Makman and E.W. Sutherland. Adenosine 3',5'-phosphate in *Escherichia coli*. *J. Biol. Chem.*, 240(3):1309–14, 1965.

S. Mangan, S. Itzkovitz, A. Zaslaver, and U. Alon. The incoherent feed-forward loop accelerates the response time of the *gal* system of *Escherichia coli*. *J. Mol. Biol.*, 356(5): 1073–1081, 2006.

G. Baptist et al. A genome-wide screen for identifying all regulators of a target gene. *Under revision*, 2012.

A.B. Oppenheim, O. Kobiler, J. Stavans, D.L. Court, and S. Adhya. Switches in bacteriophage lambda development. *Annu. Rev. Genet.*, 39:409–29, 2005.

I. Pastan and S. Adhya. Cyclic adenosine 5'-monophosphate in *Escherichia coli*. *Bacteriol. Rev.*, 40(3):527–51, 1976.

K. Potrykus, G. Wegrzyn, and V..J. Hernandez. Multiple mechanisms of transcription inhibition by ppGpp at the λ_{pR} promoter. *J. Biol. Chem.*, 277(46):4378591, 2002.

M. Reiter, B. Kirchner, H. Müller, C. Holzhauer, W. Mann, and M.W. Pfaffl. Quantification noise in single cell experiments. *Nucleids Acids Res.*, 38(18):e124, 2011.

M. Ronen, R. Rosenberg, B.I. Shraiman, and U. Alon. Assigning numbers to the arrows: Parameterizing a gene regulation network by using accurate expression kinetics. *Proc. Natl. Acad. Sci. USA*, 99(16):10555–60, 2002.

M. Slominska, P. Neubauer, and G. Wegrzyn. Regulation of bacteriophage λ development by guanosine 5'-diphosphate-3"-diphosphate. *Virology*, 262(2):431–41, 1999.

B. Volkmer and M. Heinemann. Condition-dependent cell volume and concentration of *Escherichia coli* to facilitate data conversion for systems biology modeling. *PLoS One*, 6(7): e23126, 2011.

N. Yamamoto, K. Nakahigashi, T. Nakamichi, M. Yoshino, Y. Takai, Y. Touda, A. Furubayashi, S. Kinjyo, H. Dose, M. Hasegawa, K.A. Datsenko, T. Nakayashiki, M. Tomita, B.L. Wanner, and H. Mori. Update on the Keio collection of *Escherichia coli* single-gene deletion mutants. *Mol. Syst. Biol.*, 5:335, 2009.

A. Zaslaver, A. Bren, M. Ronen, S. Itzkovitz, I. Kikoin, S. Shavit, W. Liebermeister, M.G. Surette, and U. Alon. A comprehensive library of fluorescent transcriptional reporters for *Escherichia coli*. *Nat. Methods*, 3(8):623–8, 2006.